

# Probing dark matter with star clusters: a dark matter core in the ultra-faint dwarf Eridanus II

Filippo Contenta<sup>1</sup>\*, Eduardo Balbinot<sup>1</sup>, James Petts<sup>1</sup>, Justin I. Read<sup>1</sup>, Mark Gieles<sup>1</sup>, Michelle L. M. Collins<sup>1</sup>, Jorge Peñarrubia<sup>2</sup>, Maxime Delorme<sup>1</sup>, Alessia Gualandris<sup>1</sup>

<sup>1</sup> Department of Physics, University of Surrey, Guildford GU2 7XH, UK

<sup>2</sup> Institute for Astronomy, University of Edinburgh, Royal Observatory, Blackford Hill, Edinburgh EH9 3HJ, UK

Accepted 2017 June ??; Received 2017 May ??; in original form 2017 May ??

## ABSTRACT

We present a new technique to probe the central dark matter (DM) density profile of galaxies that harnesses both the survival and observed properties of star clusters. As a first application, we apply our method to the ‘ultra-faint’ dwarf Eridanus II (Eri II) that has a lone star cluster  $\sim 45$  pc from its centre. Using a grid of collisional  $N$ -body simulations, incorporating the effects of stellar evolution, external tides and dynamical friction, we show that a DM core for Eri II naturally reproduces the size, radial light profile and projected position of its star cluster. By contrast, a dense cusped galaxy requires the cluster to lie implausibly far from the centre of Eri II ( $> 1$  kpc), with a high inclination orbit that must be observed at a particular orbital phase. Our results imply that either a cold DM cusp was ‘heated up’ at the centre of Eri II by bursty star formation, or we are seeing the first unambiguous evidence for physics beyond cold DM.

**Key words:** stars: kinematics and dynamics – globular clusters: general – galaxies: structure – galaxies: dwarf – galaxies: individual: Eridanus II – galaxies: haloes – dark matter.

## 1 INTRODUCTION

The  $\Lambda$  ‘Cold Dark Matter’ ( $\Lambda$ CDM) model gives a remarkable match to the growth of structure on large scales in the Universe (e.g. Tegmark & Zaldarriaga 2002; Planck Collaboration et al. 2014). Yet on smaller scales, inside galaxy groups and galaxies, there have been long-standing tensions (e.g. Klypin et al. 1999; Moore et al. 1999). Key amongst these is the ‘cusp-core’ problem. Pure dark matter (DM) simulations of structure formation in a  $\Lambda$ CDM cosmology predict that galaxies should reside within dense central DM cusps with density  $\rho \propto r^{-1}$  (e.g. Dubinski & Carlberg 1991; Navarro, Frenk, & White 1996b) whereas observations of the rotation curves of dwarf galaxies have long favoured constant density cores (e.g. Flores & Primack 1994; Moore 1994; Read et al. 2017). This may owe to physics beyond CDM, for example self-interacting DM (SIDM; e.g. Spergel & Steinhardt 2000; Kaplinghat et al. 2016), wave-like DM (e.g. Schive et al. 2014) or ultra-light axions (e.g. González-Morales et al. 2016). However, it is important to emphasise that all of these small-scale tensions with  $\Lambda$ CDM arise when comparing models devoid of ‘baryons’ – stars and gas – with real galaxies in the Universe. There is mounting evidence that bursty star formation during galaxy formation can ‘heat-up’ DM, transforming a DM cusp to a core (e.g. Navarro, Eke, & Frenk 1996a; Read & Gilmore 2005; Pontzen & Governato 2012, 2014;

Pontzen et al. 2015). The latest simulations – that resolve the impact of individual supernova explosions – find that DM cores, of approximately the half stellar mass radius ( $R_{1/2}$ ) in size, form slowly over a Hubble time of bursty star formation (e.g. Oñorbe et al. 2015; Read et al. 2016, hereafter R16). However, there remains disagreement in the literature over the DM halo mass scale at which such transformations become inefficient,  $M_{200} = M_{\text{pristine}}^1$ . As pointed out by Peñarrubia et al. (2012), at sufficiently low stellar mass there is no longer enough integrated supernova energy to unbind the DM cusp. Depending on the numerical scheme employed, this mass scale has been reported to be as high as  $M_{\text{pristine}} \sim 10^{10} M_{\odot}$  (e.g. Chan et al. 2015; Tollet et al. 2016) and as low  $M_{\text{pristine}} \sim 10^8 M_{\odot}$  (R16)<sup>2</sup>.

The above motivates measuring the central DM density of the very faintest galaxies in the Universe since, in a  $\Lambda$ CDM cosmology, these may be expected to retain their ‘pristine’ DM cusps (R16). There is no shortage of such faint dwarf galaxies orbiting the Milky Way, Andromeda and nearby systems (e.g. Belokurov et al. 2007; Collins et al. 2014; Bechtol et al. 2015; Sand et al. 2015). However, most of these are devoid of gas and so the kinematics of their stars must be used to probe their DM halos. This

\* Contact e-mail: f.contenta@surrey.ac.uk

<sup>1</sup>  $M_{200}$  is the virial mass. For satellite galaxies, we define this pre-infall.

<sup>2</sup> These differences result from a mix of differing numerical resolution, sub-grid physics models and how reionisation is treated. For a discussion, see Read et al. (2017).

is challenging because of a strong degeneracy between their DM density profiles and the orbit distribution of their stars (e.g. Merrifield & Kent 1990; Evans et al. 2009; Read & Steger 2017). For the brighter Milky Way dwarfs, this degeneracy can be broken by using metallicity or colour to split the stars into distinct components with different scale lengths (e.g. Battaglia et al. 2008; Walker & Peñarrubia 2011 and Agnello & Evans 2012, but see Breddels & Helmi 2013 and Richardson & Fairbairn 2014). However, for the fainter dwarfs there are too few stars to obtain strong constraints (Read & Steger 2017).

An alternative method for probing the central density of dwarf galaxies was proposed by Goerdt et al. (2006). They showed that the globular clusters (GCs) in the dwarf spheroidal galaxy Fornax would rapidly sink to the centre by dynamical friction if Fornax has a steep DM cusp. By contrast, in a constant density core, dynamical friction is suppressed (Read et al. 2006a; Inoue 2009, 2011; Petts et al. 2015, 2016), allowing Fornax’s GCs to survive through to the present day. This ‘timing argument’ was refined by Cole et al. (2012) who used 2800  $N$ -body simulations of Fornax’s GC system to show that a core is favoured over a cusp, in excellent agreement with split-population modelling of Fornax’s stars (e.g. Walker & Peñarrubia 2011). Such survival arguments were extended by Peñarrubia et al. (2009) to the GCs associated with the Sagittarius dwarf.) While it is likely that Fornax has a DM core, its stellar mass ( $M_* \sim 4 \times 10^7 M_\odot$ ; de Boer et al. 2012) is large enough for bursty star formation to drive complete cusp-core transformations (Peñarrubia et al. 2012; R16). Thus, Fornax’s core yields inconclusive constraints on the nature of DM.

In this paper, we develop a new method for measuring the central DM density of dwarf galaxies that harnesses both the survival and observed present-day properties of star clusters. Two-body relaxation is important for star clusters that are initially dense, and this causes them to expand (Hénon 1965; Gieles et al. 2010). In a tidal field, high-energy stars are pushed over the cluster’s tidal boundary, slowing down the expansion. Eventually, the cluster’s half stellar mass radius becomes a constant fraction of the tidal radius and, from that moment on, the cluster evolves at a constant density set by the tidal field (Hénon 1961; Gieles, Heggie, & Zhao 2011). Thus, the observed surface density of low-mass GCs (i.e. those that have undergone sufficient relaxation) can be used as probes of the host galaxy’s tidal field and, therefore, its density distribution (Innanen et al. 1983). This allows us to probe the DM distribution in any dwarf galaxy with low-mass star clusters, including those with a much lower stellar mass than Fornax. This is the key idea that we exploit in this work<sup>3</sup>.

To model star clusters sinking in the potential of a host dwarf galaxy, we make use of the semi-analytic dynamical friction model from Petts et al. (2016) (hereafter P16), implemented in the direct-summation code `NBODY6` (Aarseth 2003). This allows us to model the survival of star clusters, similarly to Cole et al. (2012), but with a complete  $N$ -body model of the star cluster itself, including two-body effects, binary formation and evolution and stellar evolution. By comparing a large grid of such models with observational data, we are able to constrain the DM density of dwarf galaxies that host low mass GCs, independently of timing arguments or stellar kinematic measurements.

As a first application, we apply our method to the ultra-faint

dwarf galaxy Eridanus II (Eri II) that was recently discovered by the Dark Energy Survey (DES; Bechtol et al. 2015; Koposov et al. 2015). Eri II is situated 366 kpc from the Sun, at the edge of the MW, with  $M_V = -7.1$ , a half-light radius of  $R_{1/2} = 2.31''$ , and an ellipticity of 0.48. Eri II appears to show an extended star formation history, but follow-up observations are needed to confirm this. Crnojević et al. (2016) find that Eri II has a lone star cluster at a projected distance  $\sim 45$  pc from Eri II’s centre,  $M_V = -3.5$  and a half-light radius of 13 pc (see Crnojević et al. 2016, Table 1). Compared to the MW’s star clusters (Harris 1996, 2010 edition), Eri II’s star cluster appears faint and extended, contributing just  $\sim 4\%$  of Eri II’s total luminosity.

This paper is organised as follows. In Section 2, we describe our method for probing the central DM density of dwarf galaxies using star clusters, and we motivate our priors for modelling Eri II. In Section 3, we present our main findings. In Section 4, we discuss the implications of our results for galaxy formation and the nature of DM. Finally, in Section 5, we present our conclusions.

## 2 METHOD

### 2.1 A new method for measuring the inner DM density of dwarf galaxies

We model the evolution of star clusters orbiting within a host dwarf galaxy using `NBODY6DF`. This is a publicly available (P16, [gi thub . com/JamesAPetts/NBODY6df](https://github.com/JamesAPetts/NBODY6df)) adaptation of `NBODY6`, which is a fourth-order Hermite integrator with an Ahmad & Cohen (1973) neighbour scheme (Makino & Aarseth 1992; Aarseth 1999, 2003), and force calculations that are accelerated by Graphics Processing Units (GPUs, Nitadori & Aarseth 2012). Finally, it contains metallicity dependent prescriptions for the evolution of individual stars and binary stars (Hurley et al. 2000, 2002). In `NBODY6DF`, the host dwarf galaxy is modelled as a static, analytic potential and dynamical friction is applied to star cluster members using the semi-analytic model described in P16 (see also Petts et al. 2015). The P16 model has been extensively tested against full  $N$ -body simulations of dynamical friction in both cored and cusped background potentials, giving an excellent description of the orbital decay in both cases. In particular, it is able to reproduce the ‘core-stalling’ behaviour, whereby dynamical friction is suppressed inside constant density cores (Goerdt et al. 2006; Read et al. 2006a; Inoue 2009, 2011 and see P16 for further details).

We set up a grid of 200 `NBODY6DF` simulations, varying the density profile of the galaxy (cusped or cored) and the initial orbit and properties of the star cluster. Comparing this grid with observations, we are able to determine the most likely background potential and initial star cluster properties. Since dwarf galaxies are typically dominated by DM at all radii, the background potential directly provides us with the DM density profile.

### 2.2 The DM halo of Eri II

We model the DM halo of Eri II using the coreNFW profile from R16. This is described by a mass  $M_{200}$  and concentration parameter  $c_{200}$ , identical to those used for the cusped Navarro-Frenk-White (NFW) profile (Navarro, Frenk, & White 1996b). However, it allows also for a central DM core. By default, this has a size set by the projected half light radius of the stars  $R_{1/2}$ , which for Eri II is  $R_{1/2} = 0.28$  kpc (Crnojević et al. 2016). The power-law slope of the core is set by the total star formation time  $t_{\text{SF}}$ , where  $t_{\text{SF}} = 13.8$  Gyrs

<sup>3</sup> Note that the cluster’s stellar kinematics are also affected by tides, making them additional probes of the properties of the galactic tidal field (e.g. Küpper et al. 2010; Claydon et al. 2017).

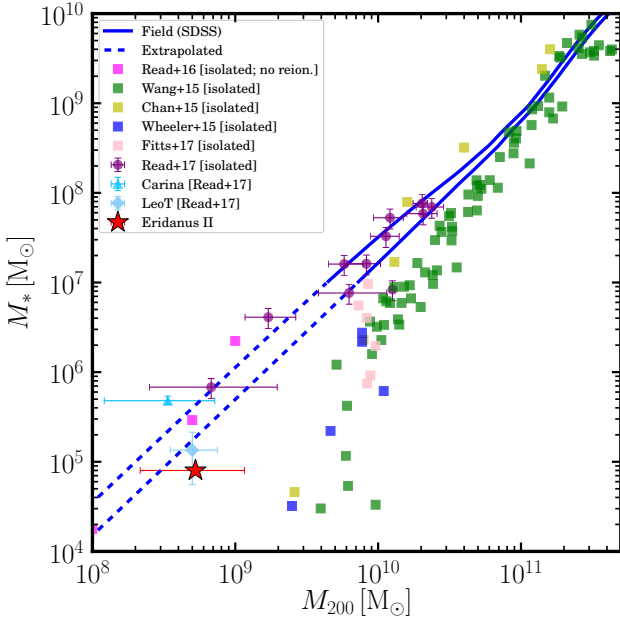


**Figure 1.** The stellar mass-halo mass relation of isolated dwarf galaxies. The symbols correspond to the observational data and the squares to the results from  $N$ -body simulations. The blue solid lines show the results from abundance matching in  $\Lambda$ CDM using the SDSS field stellar mass function (where the lines are dashed, the results are extrapolated). Eri II is marked by the red star. It appears to be consistent with a ‘failed’ Leo T, inhabiting a similar DM halo but having its star formation shut down earlier, lowering its  $M_*$  for the same pre-infall  $M_{200}$ .

produces a flat dark matter core, while  $t_{\text{SF}} = 0$  Gyrs returns the fully cusped NFW profile.

Eri II’s stellar population may be expected to be like other similar stellar mass dwarf galaxies (e.g. Bootes I and Ursa Major I; see McConnachie 2012). These have predominantly old-age stars. Santana et al. (2013) showed that the apparent intermediate-age population in these galaxies is likely due to the presence of blue straggler stars. However, they could not rule out the presence of an intermediate-age population of up to 3 Gyr old. Recent HST data (propID 14234; subject of a future publication), has confirmed that Eri II’s stellar population is similar to those studied by Santana et al. (2013), hence favoring an older population. In this work, we choose to be conservative and consider two extremes: no core formation ( $t_{\text{SF}} = 0$ ) and ‘maximal’ core formation ( $t_{\text{SF}} = 9$  Gyrs), meaning that we allow  $t_{\text{SF}}$  to be as large as possible given current observational constraints. We stress, however, that the precise value of  $t_{\text{SF}}$  should not be over-interpreted. It is calibrated on the idealised simulations of isolated dwarfs in R16 that do not explore the cosmological evolution of halos, scatter in the DM halo concentration and spin parameters, or the effect of reionisation. All of these could break the simple correspondence between  $t_{\text{SF}}$  and the DM core size. We discuss this further in Section 4.

To obtain an estimate of the (pre-infall) halo mass,  $M_{200}$ , for Eri II we use the recent measurement of its mass within the half light radius  $M_{1/2} = 1.2^{+0.4}_{-0.3} \times 10^7 M_{\odot}$ , derived from stellar kinematics by Li et al. (2017). We turn this into an  $M_{200}$  by fitting an NFW profile to  $M_{1/2}$  using the  $M_{200} - c_{200}$  relation from Macciò et al. (2007), finding  $M_{200} = 4.7^{+6.9}_{-2.6} \times 10^8 M_{\odot}$ .

To test if the above value for  $M_{200}$  is reasonable, in Fig. 1 we

compare the stellar mass ( $M_* \simeq 8 \times 10^4 M_{\odot}$ ; Bechtol et al. 2015) and  $M_{200}$  for Eri II with measurements for other nearby dwarfs; Eri II is marked by the red star. The magenta diamonds show the  $M_* - M_{200}$  relation for isolated gas rich dwarfs from Read et al. (2017). The dark cyan triangle shows a measurement for the Carina dwarf spheroidal galaxy from Ural et al. (2015). The light cyan diamond shows an estimate for the isolated dIrr Leo T from Read et al. (2017). The blue solid and dashed lines show the  $M_* - M_{200}$  relation derived by Read et al. (2017) from abundance matching in  $\Lambda$ CDM using the SDSS field stellar mass function (the dashed lines show where this is extrapolated). The remaining data points show the latest results from a range of simulations of isolated dwarfs taken from the literature: R16 (magenta); Wang et al. (2015) (green); Chan et al. (2015) (yellow); Wheeler et al. (2015) (blue); and Fitts et al. (2016) (pink). As can be seen, there is a clear discrepancy between most simulations and the data below  $M_{200} \sim 10^{10} M_{\odot}$  that remains to be understood. For our paper here, however, this plot demonstrates that our derived  $M_{200}$  for Eri II is in good agreement with estimates for other galaxies of a similar stellar mass. Eri II is consistent with a ‘failed’ Leo T, inhabiting a similar DM halo but having its star formation shut down earlier, lowering its  $M_*$  for the same pre-infall  $M_{200}$ . This is further evidenced by the lack of detected HI gas, or recent star formation, in Eri II (Crnojević et al. 2016).

In Fig. 2, we show the cumulative mass profiles (left panel) and DM density profiles (right panel) for Eri II that we assume in this work. The grey lines show the cusped model, the green lines show the cored model. The middle of the three lines shows  $M_{200} = 5 \times 10^8 M_{\odot}$  that we assume from here on. The top and bottom lines show the upper and lower boundary of  $M_{200}$  estimated from the kinematic measurements (Li et al. 2017). The projected half light radius of the stars,  $R_{1/2}$ , is marked by the vertical blue line. On the right panel, the measurement of  $M_{1/2}$  for Eri II from Li et al. (2017) is marked by the red data point. As can be seen, due to the  $M_{200} - c_{200}$  relation, changing  $M_{200}$  produces only a small effect on the DM density within  $R_{1/2}$ . Thus, our method will not be sensitive to  $M_{200}$ . (This is why we must constrain  $M_{200}$  using the stellar kinematic data.) However, cusped and cored models look very different within  $R_{1/2}$  and this is what we aim to probe in this work.

Finally, the latest version of `NBODY6DF` only supports a background DM density profile modelled by Dehnen spheres (Dehnen 1993):

$$\rho(r) = \frac{M_0(3-\gamma)}{4\pi r_0^3} \left(\frac{r}{r_0}\right)^{-\gamma} \left(1 + \frac{r}{r_0}\right)^{\gamma-4}, \quad (1)$$

where  $M_0$  and  $r_0$  are the mass and scale length, respectively, and  $-\gamma$  is the logarithmic slope of the inner density profile.

Thus, to obtain DM profiles suitable for `NBODY6DF`, we fit the above Dehnen profile to our coreNFW density profiles. These fits are shown by the dashed lines in the right panel of Fig. 2. As can be seen, inside  $R_{1/2}$  (our region of interest), these fits are excellent. Our best-fit parameters for the cored ( $\gamma = 0$ ) and cusped ( $\gamma = 1$ ) models were:  $M_0 = 4.79 \times 10^8 M_{\odot}$  and  $r_0 = 0.877$  kpc and  $M_0 = 2.94 \times 10^8 M_{\odot}$  and  $r_0 = 1.078$  kpc, respectively.

### 2.3 Eri II’s star cluster

We model the initial conditions of Eri II’s star cluster as a Plummer sphere (Plummer 1911) with a Kroupa IMF (Kroupa 2001), sampling stars with masses between  $0.1 M_{\odot}$  and  $100 M_{\odot}$  and assuming a metallicity of  $Z = 0.0008$  (corresponding to  $[\text{Fe}/\text{H}] \simeq -1.5$ ). We

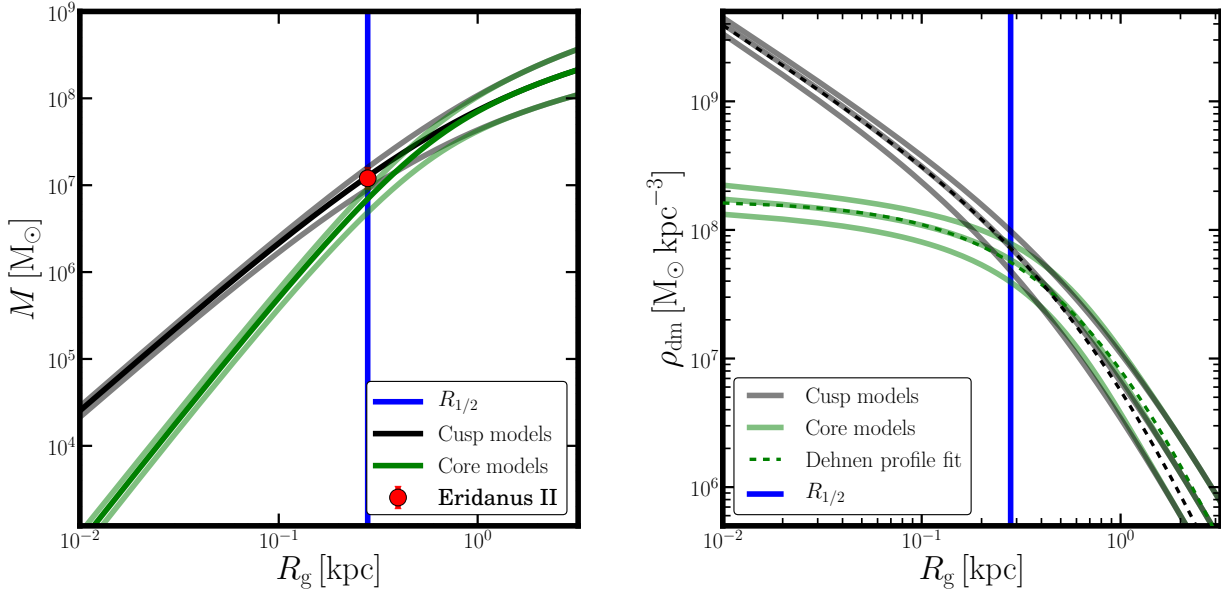


**Figure 2.** DM halo models for Eri II, chosen as described in Section 2.2. The left panel shows the cumulative mass profiles; the right panel the logarithmic density profiles. The mass within the projected stellar half light radius  $M_{1/2}$  is marked by the red data point with error bars on panel a (taken from (Li et al. 2017)). The dashed black and green lines show the cusped and cored models explored in this work, respectively. These are the best-fit Dehnen profile models to the dwarf galaxy models marked by the solid black and green lines, respectively. We explore here only a DM halo with a virial mass of  $5 \times 10^8 M_\odot$ . The halo mass of the upper and lower cusp profiles (shaded black lines) in panels a and b are derived from Eri II’s stellar kinematics (Li et al. 2017). For the core profiles, we used the same halo mass of the cusp profiles and assumed a  $t_{SF} = 9$  Gyr. The vertical blue line on both panels marks the projected half light radius of Eri II,  $R_{1/2}$ .

assumed a range of initial masses  $M_{cl,0}$  and half-mass radii  $r_{hm,0}$  for the cluster to explore how its initial properties impact its final state.

## 2.4 Exploring parameter space

To explore the parameter space, we ran 200 simulations, 100 for each galaxy model (core and cusp). We varied  $r_{hm,0}$ ,  $M_{cl,0}$  and the initial galactocentric distance ( $R_{g,0}$ ) of the cluster. We allowed the cluster to have a  $r_{hm,0}$  of 1, 5, 10, 15 and 20 pc; a  $M_{cl,0}$  of approximately 13,000, 19,000, 25,000 and 32,000  $M_\odot$ ; and  $R_{g,0}$  of 0.14, 0.28, 0.56, 1.12 and 2.8 kpc. The  $r_{hm,0}$  range is based on what is found for young massive clusters (Portegies Zwart et al. 2010). The minimum  $M_{cl,0}$  is chosen such that after stellar mass loss the mass is always above the mass of the cluster. The maximum mass was chosen such that less than 20% of all stars in the entire galaxy originated from the star cluster, which is a reasonable upper limit (Larsen et al. 2012, 2014).

For all clusters we adopted circular orbits. This favours the survival of clusters in cusped profiles because eccentric orbits reach closer to the centre of the galaxy where clusters are less likely to survive. (Our assumption that the host dwarf galaxy has a spherical potential similarly favours a cusped profile because in triaxial models there are no circular orbits and only the more damaging radial orbits are allowed.)

Contenta et al. 2017 show how the observations of faint star clusters - like Eri II’s star cluster - can be affected by primordial binaries and the retention fraction of black holes, together with observational biases. In our simulations we did not vary these aspects, nor did we vary the initial density profile of the clusters. However, we expect that these aspects affect the evolution of the clusters in the cusped and cored models in the same way.

Eri II’s star cluster is observed at a projected distance  $D_g^{cl} = 45$  pc from the centre of Eri II. Thus we also need to take into account the probability for the cluster to be observed at that radius in the total likelihood. We estimate the probability  $P(D_g < D_g^{cl} | R_g)$  to observe a cluster (on a circular orbit) within  $D_g^{cl}$  for a given  $R_g$ , assuming a random inclination of the orbital plane with respect to the observer. To compute  $P(D_g < D_g^{cl} | R_g)$ , firstly we estimate the angle  $\varphi(i, R_g)$ , which defines the angle in which the cluster is observed to be within  $D_g^{cl}$  during 1/4 of an orbit (see Fig. 3), where  $i \in [0, \pi/2]$  is the angle between the pole of the orbit and the line of sight. For circular orbits, the angle  $\varphi(i, R_g)$  is given by

$$\varphi(i, R_g) = \begin{cases} \frac{\pi}{2} - \arcsin\left(\frac{\sqrt{1 - D_g^{cl}/R_g}}{\sin i}\right), & R_g > D_g^{cl}, \\ \frac{\pi}{2}, & R_g < D_g^{cl}. \end{cases} \quad (2)$$

Secondly, we integrate  $\varphi(i, R_g)$  with respect to  $\cos i$ , because for random inclinations of the orbital plane,  $\cos i$  is uniformly distributed. We then divide by a normalization angle,  $\pi/2$ , because  $\varphi(i, R_g)$  considers only 1/4 of an orbit, see Fig. 3 and we obtain

$$P(D_g < D_g^{cl} | R_g) = \frac{2}{\pi} \int_0^1 \varphi(i, R_g) d \cos i. \quad (3)$$

By definition  $0 \leq P(D_g < D_g^{cl} | R_g) \leq 1$ .

To compare the  $N$ -body simulations with the observational data, we assumed a stellar mass-to-light ratio of  $M/L_V = 2$ , appropriate for old, metal-poor stellar populations (e.g. McLaughlin & van der Marel 2005), obtaining  $M_{ob} = 4.3 \times 10^3 M_\odot$ . We multiply the observed half-light radius ( $r_{hl}$ ) by 4/3 to correct for projection

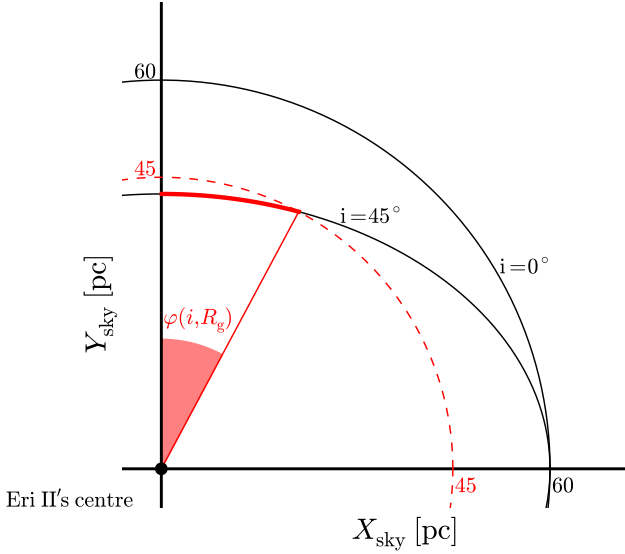


**Figure 3.** Schematic representation of two projected orbits with different inclinations of their orbital plane  $i$  (solid black lines). Eri II’s cluster is observed to be 45 pc from the centre of Eri II in projection (dashed red line). We consider that a cluster can be observed as Eri II’s star cluster if its orbit is within 45 pc (solid red line). For a given  $i$ , a larger distance from the centre results in a smaller  $\varphi(i, R_g)$  (see equation 2). Therefore, clusters that orbit in the outskirts of Eri II are unlikely to be observed near the centre.

effects (Spitzer 1987), to get an estimate for the 3D half-mass radius  $r_{h,ob} = 17.3 \text{ pc}^4$  of Eri II’s star cluster. To find the model that best fit the observational data, we maximise the likelihood for the fitting parameters ( $r_{hm,0}$ ,  $M_{cl,0}$ , and  $R_{g,0}$ ). The log-likelihood function is:

$$\ln \mathcal{L} = -\frac{(r_{h,ob} - r_{hm})^2}{2\sigma_r^2} - \frac{\log^2(M_{ob}/M_{cl})}{2\sigma_{\log(M)}^2} + \ln P(D_g < D_g^{cl}|R_g), \quad (4)$$

where  $\sigma_r = 1.33 \text{ pc}$  and  $\sigma_{\log(M)} = 0.24^5$  are the uncertainties derived from the observation (Crnojević et al. 2016). The last term in the equation above is given by equation (3) and acts as a prior to our likelihood given that it penalises models that are less likely to be observed simply due to geometrical constraints.

Therefore, by computing  $r_{hm}$ ,  $M_{cl}$  (sum of the mass of all the particles within the tidal radius of the cluster) and  $R_g$ , we can find the likelihood with equation (4) for each output time of the simulation.

## 2.5 Estimation of the number density profile

To study the structural properties of the clusters in the  $N$ -body simulations, we used a maximum likelihood fit following the procedure described in Martin et al. (2008). We model the distribution of the stars of the clusters with two-dimensional elliptical Plummer and spherical, single-component King models (King 1966). We fit the models with a Monte Carlo Markov Chain (MCMC) method

(EMCEE code, Foreman-Mackey et al. 2013) to optimize the following parameters: projected half-number radius, ellipticity, position angle, and surface density background for the Plummer models; and half-number radius, central dimensionless potential and background surface density for the King models<sup>6</sup>.

## 3 RESULTS

### 3.1 Cusp vs. core

The main result of our investigation is that the presence of a cored DM profile in Eri II allows a star cluster to not only survive in the centre of the galaxy, but also to expand up to  $r_{hm} \approx 17 \text{ pc}$  (i.e.  $r_{hl} \approx 13 \text{ pc}$ ), in excellent agreement with observations of Eri II’s lone star cluster. By contrast, a cusped DM profile gives a poorer fit overall and requires special conditions that have to be satisfied. In Fig. 4, we show a schematic representation of a simulated cluster in a cusped galaxy (on the left) and a cored galaxy (on the right) at times when they best reproduce the observations (shown in the middle). As can be seen, in the cored galaxy (right), the star cluster (green) stalls at a radius  $\sim 45 \text{ pc}$  from Eri II’s centre (see the zoomed image in the blue circle that shows its orbital decay and stalling in red). In this case, no special inclination or time are required to reproduce Eri II’s star cluster. Notice also that the cluster appears visibly extended, similarly to Eri II’s cluster, and that it shows little to no tidal tails, as expected for a cluster orbiting in a constant density core (e.g. Petts et al. 2016). By contrast, in the cusped case (left), the cluster must orbit much farther ( $R_g > 1 \text{ kpc}$ ) from Eri’s centre in order to survive. Now it’s orbit will only be close enough to Eri II in projection when the red circle lies inside the two solid yellow lines. This happens when the cluster orbits with a high inclination ( $i > 87.43^\circ$ ) of the orbital plane, and is in a particular orbital phase (fraction of the orbit  $< 3$  per cent). In the cusped galaxy, the cluster is denser than in the cored case and less consistent with the data for Eri II’s cluster. There are also now two visible tidal tails, as expected for a cluster orbiting in a cusped background.

In Fig. 5, we show the maximum likelihood of our models as a function of  $R_{g,0}$ , varying all the other parameters ( $M_{cl}$ ,  $r_{hm}$ , and  $t$ ), without (left) and with (middle)  $P(D_g < D_g^{cl}|R_g)$  in the likelihood; and as a function of time,  $t$  (varying all the other parameters and including  $P(D_g < D_g^{cl}|R_g)$ , right). The shaded grey and green regions show the 68% confidence intervals for the parameters  $R_{g,0}$  and  $t$  for the cusped (grey) and cored (green) galaxy, respectively. (Assuming that the Wilks’ theorem is valid, we used the likelihood ratio to estimate the confidence intervals (Wilks 1938); we do not allow our reported confidence interval to be smaller than the distance between two data points.)

For the clusters in the cored galaxy, the likelihood is bimodal because it is possible to fit the data if the cluster is either in the inner or outer region of the galaxy (see the left panel). For  $R_{g,0} = 0.56 \text{ kpc}$ , the tidal radius of the cluster is close to its minimum and there it is more difficult to increase the cluster’s  $r_{hl}$  up to the observed 13 pc. This leads to the dip in the likelihood at this point. However, including the probability  $P(D_g < D_g^{cl}|R_g)$  of observing the cluster at the right position (middle panel) breaks this bimodality, favouring the orbits near the centre with lower  $R_{g,0}$ .

<sup>4</sup> Assuming that light traces mass, which is not necessarily true if the cluster is mass segregated.

<sup>5</sup>  $\sigma_r$  is the uncertainties on the 3D half-mass radius; while  $\sigma_{\log(M)}$  is estimated assuming  $M/L_V = 2$ .

<sup>6</sup> We used the LIMEPY code (Gieles & Zocchi 2015) to compute the projected density profiles of King models (<https://github.com/mgieles/limepy>).



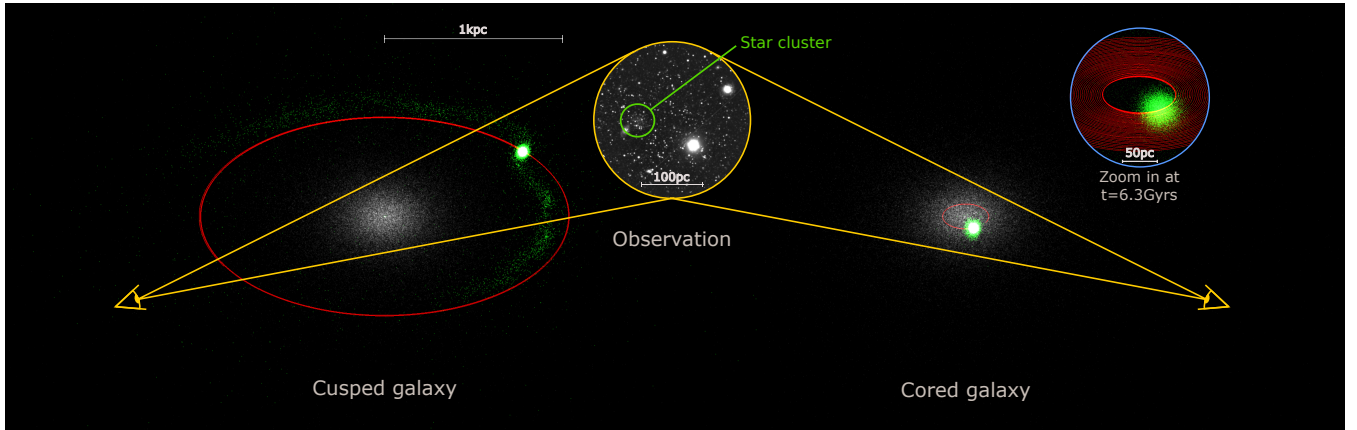


**Figure 4.** Schematic representation of the cluster orbiting in a cusped Eri II (on the left) and a cored Eri II (on the right) at times when they best reproduce the observations (Crnojević et al. 2016; shown in the middle). On the top right, we show a zoom-in of the simulation in the cored galaxy after 6.3 Gyr. The effect of dynamical friction and stalling can be seen in the red lines that depict the cluster’s orbit. In the cusped case, the cluster can only survive in the outskirts of Eri II, while in the cored case the cluster can survive in the central region where it is much more likely to match the observations.

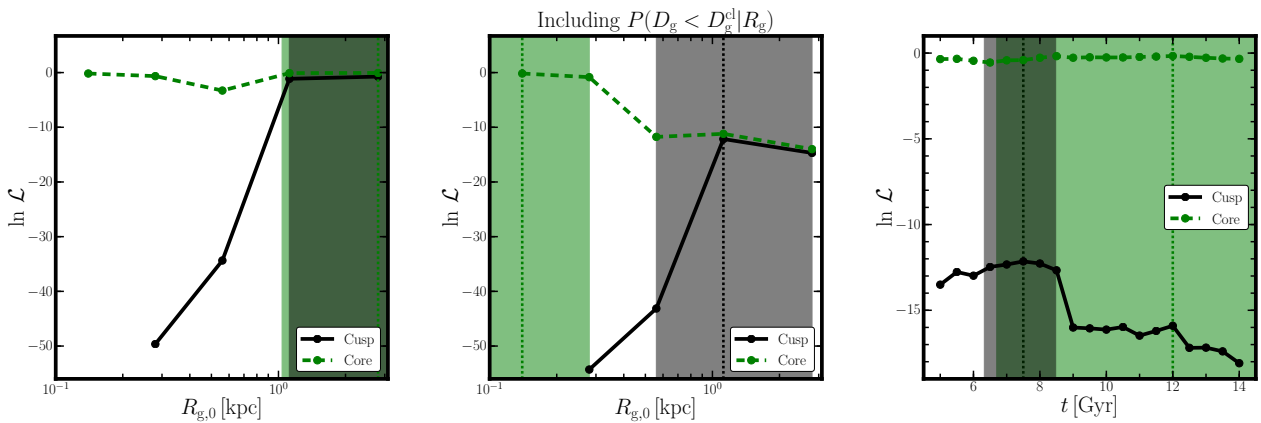


**Figure 5.** Comparison of the maximum likelihood of the cored and cusped  $N$ -body models. The left and middle panels show the maximum likelihood as a function of the initial value of  $R_g$  ( $R_{g,0}$ ) without (left) and with (middle)  $P(D_g < D_g^{\text{cl}} | R_g)$ . The right panel shows the maximum likelihood as a function of time,  $t$ , also with  $P(D_g < D_g^{\text{cl}} | R_g)$ . The black solid and green dashed lines are for cusp and core models, respectively. The shaded areas show the 68% confidence intervals for  $R_{g,0}$  and  $t$  for the cored (in green) and cusped (in black) models. The dotted vertical lines show the best-fit values for  $R_{g,0}$  and  $t$ . Notice that the cored models have a higher likelihood than the cusped models, especially once the probability of observing the cluster at its current projected distance,  $P(D_g < D_g^{\text{cl}} | R_g)$ , is included.

For the clusters evolving in the cusped galaxy, no star cluster can survive in the inner galaxy  $R_{g,0} < R_{1/2}$  for more than 5 Gyrs and the likelihood is, therefore, zero for all clusters in that region of parameter space chosen in this study. Considering more massive clusters initially does not necessarily lead to higher probability of survival, because of the increased importance of dynamical friction. Clusters that orbit outside the scale radius ( $R_{g,0} \gtrsim 1$  kpc) have comparable likelihoods in the cusped and cored models (see left and middle panels) because they are similar by construction at large radii (compare the green and black dashed lines in the right panel of Fig. 2). A measurement of the 3D position of the cluster in Eri II would allow us to rule out cusped models. However, to measure a 1 kpc offset from Eri II, an accuracy of 0.006 mag is needed. Even with RR Lyrae, it is only possible at present to reach an accuracy of 0.05 mag.

The right panel of Fig. 5 shows the maximum likelihood at different times. The black line is for clusters in a cusped galaxy, for

which the best fits are the models between 6.5 and 8 Gyr old. The green dashed line is for the cored DM profile, for which the best fits are all models with  $t \gtrsim 7$  Gyr. In the cored galaxy, the best fit models are those that survive in the inner part of the galaxy where they can easily expand up to  $\sim 17$  pc and survive for 14 Gyr. For the cusped galaxy, we can only reproduce the observed properties of Eri II star cluster for a small amount of time and for a small range of  $M_{\text{cl},0}$  and  $r_{\text{hm},0}$ . To reproduce Eri II’s star cluster in a cusped galaxy, it must therefore have an age of 6.5 – 8 Gyr. This provides another prediction to further test our result.

Finally, even if we accept a high inclination of the orbital plane and the required orbital phase for the cusped case, its star clusters give a poorer fit to the observations than the cored case, because the clusters are not able to expand as much. We discuss this in more detail next.

### 3.2 Best-fit star cluster models

The best-fit model in the cusped galaxy has  $M_{\text{cl},0} \sim 3.2 \times 10^4 M_{\odot}$ ,  $r_{\text{hm},0} = 5$  pc, and  $R_{\text{g},0} = 1.12$  kpc. The best-fit model in the cored galaxy has  $M_{\text{cl},0} \sim 1.9 \times 10^4 M_{\odot}$ ,  $r_{\text{hm},0} = 10$  pc, and  $R_{\text{g},0} = 0.14$  kpc. Fig. 6 shows the evolution of  $M_{\text{cl}}$ ,  $r_{\text{hm}}$ ,  $R_{\text{g}}$  and  $P(D_{\text{g}} < D_{\text{g}}^{\text{cl}} | R_{\text{g}})$  for these two models. The red shaded areas show the 68% confidence intervals of the data. (We only have a lower limit for the age of the cluster, because stars younger than 5 Gyr have not been observed; see Section 1.) In Fig. 6, we show that the properties of the star cluster in a cored DM profile reproduce the properties of the observed star cluster for all times  $\gtrsim 5$  Gyr, while in the cusped case the cluster has to be observed at a specific time. Notice, however, that the cusped model is always at tension with the data, with its size,  $r_{\text{hm}}$ , never quite reaching high enough to match Eri II's star cluster.

As discussed in Section 1, we expect the density of the star cluster to reach an equilibrium due to relaxation-driven expansion and the tidal pruning of high-energy escaper stars. In the left panel of Fig. 6, we see this process happening between 5 and 9 Gyr for the cusped model. Over this period, the cluster evolves at an approximately constant  $r_{\text{hm}}/r_{\text{J}}$  (Hénon 1961), where  $r_{\text{J}}$  is the ‘Jacobi’ or tidal radius. As a result, the cluster shrinks as  $r_{\text{hm}} \propto M^{1/3}$  while it loses mass, and it only has a large  $r_{\text{hm}}$  for a limited time (few Gyrs). The cluster in the cored galaxy also expands, but  $\gtrsim 5$  Gyrs the star cluster evolves at roughly constant  $M_{\text{cl}}$  and constant  $r_{\text{hm}}$ . This is because the escape rate is very small in compressive tides, and the cluster evolves towards a near isothermal equilibrium configuration, in which the cluster is in virial equilibrium with the tides (Yoon, Lee, & Hong 2011; Bianchini et al. 2015 Webb, Patel, & Vesperini 2017). This implies that it is more likely to find a cluster in this phase, because it can be in this quasi-equilibrium configuration for a long time ( $\gtrsim 10$  Gyrs). The asymptotic value of  $r_{\text{hm}}$  of the cluster in the cored galaxy is in excellent agreement with the data for Eri II's star cluster (red shaded region). We note that in our  $N$ -body model the cluster density within  $r_{\text{hm}}$  evolves to approximately the same value as the (uniform) DM density, hence the cluster density is literally probing the DM density.

### 3.3 Predicted cluster number density profiles

Fig. 7 shows the stellar number density profiles of the best-fit models in the cusped (left) and cored (right) case. Crnojević et al. (2016) find the structural parameters of Eri II's star cluster by fitting a Sersic profile to its surface brightness as measured from integrated photometry. It is possible to similarly derive a surface brightness profile from the  $N$ -body simulations, however it proved challenging to directly compare the models to the data. Analysing the image from (Crnojević et al. 2016), we found that the result is very sensitive to the number of bins used, the subtraction of background sources and which bright stars are masked – all of which can change the result of the fitting. Therefore, for our analysis we used a different approach in which the data from the  $N$ -body models are not binned. We used only bright stars (massive stars) that are observable. In our case, we chose only stars that are more massive than  $0.75 M_{\odot}$ <sup>7</sup>. Furthermore, we included the background stars using the number density profile of Eri II reported in (Bechtol et al. 2015), assuming that the stars are uniformly distributed in our simulated field of view.

As can be seen in Fig. 7, a star cluster that evolves in a DM cusp has a different density profile than a star cluster that evolves in a DM core. In the cored galaxy, clusters have a lower concentration parameter,  $c = 0.55 \pm 0.16$ , compared to the cluster in the cusped galaxy ( $c = 0.83 \pm 0.07$ ). Here  $c \equiv \log(r_{\text{t}}/r_0)$ , where  $r_{\text{t}}$  is the truncation radius and  $r_0$  is the King/core radius. This means that the core of the cluster is larger (for a given  $r_{\text{hl}}$ ) if it evolves in a DM core. From deeper imaging, it may be possible to derive the projected density profile of the cluster, allowing for a better comparison with our  $N$ -body simulations.

## 4 DISCUSSION

Our key result is that we find a DM core in the ultra-faint dwarf galaxy Eri II. Our mass model for Eri II has a DM core size set by the projected half light radius of the stars  $R_{1/2} \sim 0.28$  kpc (see Fig. 2). However, the data only require that there is a dark matter core where we see Eri II's star cluster today. This sets a minimum core size of  $r_{\text{core}} > 45$  pc. In this section, we explore what such a dark matter core means for galaxy formation and the nature of dark matter.

### 4.1 Dark matter heating

The DM core we find in Eri II is in excellent agreement with predictions from the ‘DM heating’ model of R16 if star formation in Eri II continued for  $t_{\text{SF}} = 9$  Gyr. However, as discussed in Section 1, the star formation time of Eri II is likely substantially shorter than this. This may point to an inability for bursty star formation to form the DM core in Eri II, perhaps pointing to beyond- $\Lambda$ CDM physics. But we should be wary of over-interpreting the parameter  $t_{\text{SF}}$ . The R16 simulations are of idealised isolated ‘cooling halos’. They do not model the cosmological growth of dwarf galaxy halos, their scatter in concentration and spin parameters, nor the effect of reionisation. These will all act to complicate the relationship between dark matter cores and the observed properties of dwarf galaxies. Indeed, both Madau et al. (2014) and Oñorbe et al. (2015) find in their fully cosmological simulations that significant DM cores can form early<sup>8</sup>.

For these reasons, following Peñarrubia et al. (2012), R16 and Read et al. (2017), we focus on the energy required to unbind Eri II's dark matter cusp:

$$\frac{\Delta E}{\Delta W} = \frac{M_{\star}}{\langle m_{\star} \rangle \Delta W} \xi \epsilon_{\text{DM}} \quad (5)$$

where  $\Delta E$  is the total integrated supernova energy,  $\Delta W$  is the energy required to unbind the dark matter cusp,  $M_{\star}$  is the stellar mass,  $\langle m_{\star} \rangle = 0.83$  is the mean stellar mass,  $\xi = 0.00978$  is the fraction of mass in stars that go supernova (i.e. those with mass  $m_{\star} > 8 M_{\odot}$ ), and  $\epsilon_{\text{DM}} = 0.0025$  is the coupling efficiency of the SNe energy to the dark matter. (We assume a Chabrier initial stellar mass function (IMF; Chabrier 2003) over the stellar mass range  $0.1 < m_{\star}/M_{\odot} < 100$ , and estimate  $\epsilon_{\text{DM}}$  using the simulations in R16.)

In Fig. 8, we plot  $\Delta E/\Delta W$  as a function of the DM core size  $r_{\text{core}}$ . The horizontal dashed line marks  $\Delta E/\Delta W = 1$ . Above this line, there is enough integrated supernova energy to unbind the

<sup>7</sup> This mass limit was derived from the observational limit reported in Crnojević et al. (2016) and PARSEC's isochrones v1.2S (Bressan et al. 2012)

<sup>8</sup> Further complications can arise following the minor mergers of star-free subhalos. These can even cause DM cusps to regrow (Laporte & Peñarrubia 2015).

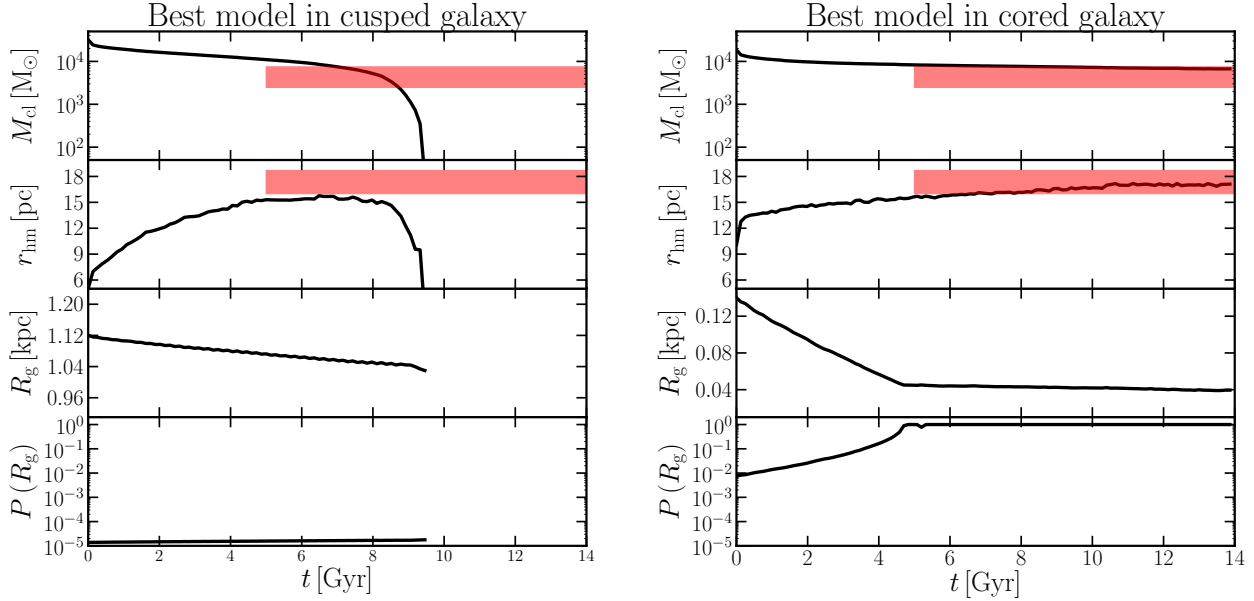


**Figure 6.** (a): Evolution of  $M_{cl}$ ,  $r_{hm}$ ,  $R_g$  and the probability to observe a cluster in projection at  $D_g \leq 45$  pc, for the best-fit cusped model. Right panel: as left panel but for the best-fit cored model. The red shaded regions show the 68% confidence intervals of the data. (We only have a lower limit for the age of the cluster, because stars younger than 5 Gyr have not been observed; see Section 1.)

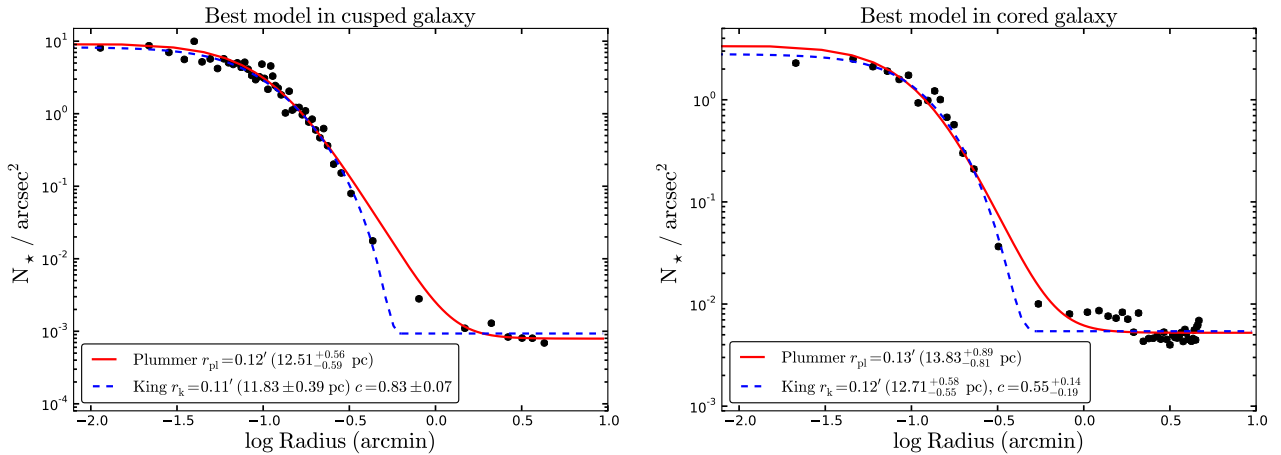


**Figure 7.** (a): Number density profile of the best cusp model at 7.5 Gyr. (b): Number density profile of the best core model at 12 Gyr. The solid red and dashed blue lines indicate the best fit Plummer and King profiles, respectively. The number density of background star is estimated using the number density profile of Eri II (Bechtol et al. 2015). On the right, the number of background stars is higher because the cluster sits in the inner part of Eri II.

cusp; below there is insufficient energy. The vertical green line marks the minimum core size,  $r_{core,min} = 45$  pc set by the current projected position of Eri II's star cluster. The vertical blue line marks the core size assumed in this work,  $r_{core} = R_{1/2} = 0.28$  kpc. The black and orange shaded regions assume a DM halo mass of  $M_{200} = 5 \times 10^8 M_\odot$  with a stellar mass  $M_* = 8.3^{+5.1}_{-4.2} \times 10^4 M_\odot$  (Bechtol et al. 2015, assuming three times their uncertainties), and a concentration parameter of  $c_{200} = 23$  and  $c_{200} = 14$ , respectively. These are the upper and lower 68% confidence intervals of  $c_{200}$  in  $\Lambda$ CDM (Dutton & Macciò 2014). (Note that the R16 simulations assume the upper envelope of this  $c_{200}$  range and so make core formation maximally difficult.)

As can be seen in Fig. 8, there is plenty of energy to produce

the minimum core size  $r_{core} = 45$  pc independently of the assumed  $c_{200}$  or  $M_*$ . However, for the assumed DM halo mass and supernova energy coupling efficiency that we assume here, a low  $c_{200}$  and high  $M_*$  for Eri II are required to produce a core as large as  $r_{core} = R_{1/2} = 0.28$  kpc.

While the R16 models are able to produce a DM core in Eri II, most other simulations in the literature to date do not find DM cores in halos below  $M_{200} \sim 7.5 \times 10^9 M_\odot$  (e.g. Oñorbe et al. 2015; Chan et al. 2015; Tollet et al. 2016, but see Madau et al. 2014). We can understand the origin of this discrepancy from Fig. 1. As can be seen, the R16 simulations (magenta squares) produce a similar total stellar mass to the Chan et al. (2015) (yellow squares) and Wang et al. (2015) (green squares) simulations but in halos



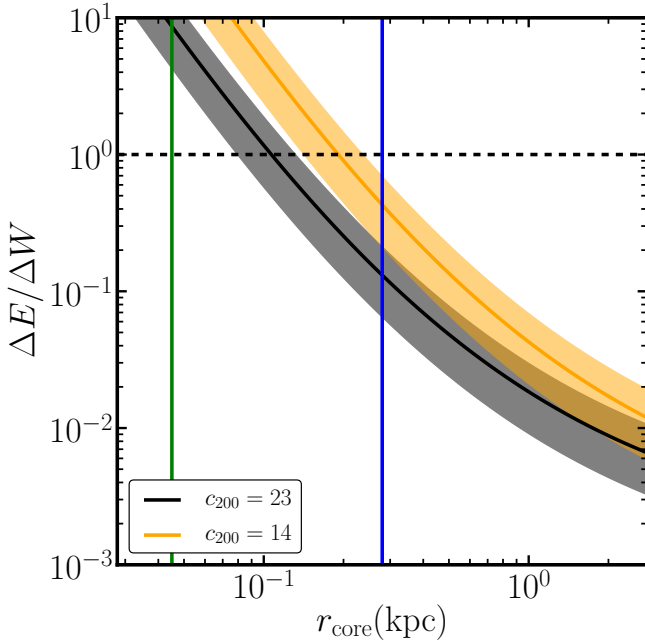


**Figure 8.** The energy required to unbind Eri II’s DM cusp as a function of the DM core size,  $r_{\text{core}}$ . We assume for this plot a Chabrier IMF (Chabrier 2003) and a coupling efficiency between supernovae and dark matter of  $\epsilon_{\text{DM}} = 0.25\%$  (R16). The horizontal dashed line marks  $\Delta E/\Delta W = 1$ . Above this line, there is enough integrated supernova energy to unbind the cusp; below there is insufficient energy. The vertical green line marks the minimum core size,  $r_{\text{core,min}} = 45$  pc set by the current projected position of Eri II’s star cluster. The vertical blue line marks the core size assumed in this work,  $r_{\text{core}} = R_{1/2} = 0.28$  kpc. The black and orange shaded regions assume a DM halo mass of  $M_{200} = 5 \times 10^8 M_{\odot}$  with a stellar mass  $M_{*} = 8.3^{+5.1}_{-4.2} \times 10^4 M_{\odot}$  (Bechtol et al. 2015, assuming three times their uncertainties), and a concentration parameter of  $c_{200} = 23$  and  $c_{200} = 14$ , respectively. These are the upper and lower 68% confidence intervals of  $c_{200}$  in  $\Lambda$ CDM (Dutton & Macciò 2014).

an order of magnitude lower in mass. (Note that the Wang et al. (2015) simulations are the same as those discussed in Tollet et al. (2016).) This is why cusp-core transformations in the R16 simulations are energetically feasible. The simulations that find no cores below  $M_{200} \sim 7.5 \times 10^9 M_{\odot}$  form almost no stars below this mass scale and so do not have enough integrated supernova energy to unbind the dark matter cusp (see also the discussion in Read et al. 2017). Understanding this apparent discrepancy between the data and simulations in Fig. 1, and the differences between numerical models, remains an open and important problem.

If Eri II is found to have a purely old stellar population, with too few supernovae to provide the energy required to unbind its cusp, then we will be forced to move to models beyond  $\Lambda$ CDM. We consider some of these, next.

## 4.2 Beyond $\Lambda$ CDM

The small scale puzzles in  $\Lambda$ CDM (see Section 1) have motivated the community to consider alternative models. Some of these can solve the cusp-core problem without recourse to baryonic ‘dark matter heating’. The most popular of these to date is Self-Interacting Dark Matter (SIDM; Spergel & Steinhardt 2000). The latest SIDM models have a velocity-dependent interaction cross

section  $\sigma/m(v/v_m)$ , where  $\sigma$  is the dark matter interaction cross section,  $m$  is the mass of the dark matter particle and  $v_m$  is a velocity scale (e.g. Kaplinghat et al. 2016; Schneider et al. 2016). This is required for the models to be consistent with constraints from weak lensing on galaxy cluster scales that favour  $\sigma/m < 0.5 \text{ cm}^2/\text{g}$  (e.g. Harvey et al. 2015), while maintaining a much higher  $\sigma/m \sim 2\text{--}3 \text{ cm}^2/\text{g}$  required to produce dark matter cores in dwarf galaxies. Schneider et al. (2016) present a simple model for the relationship between the DM core size and the self interaction cross section. Assuming  $v_m = 30 \text{ km/s}$  and a mass for Eri II of  $M_{200} = 5 \times 10^8 M_{\odot}$ , we obtain from their figure 9:

$$r_{\text{core}} \sim 0.315 \left( \frac{\sigma/m}{1 \text{ cm}^2/\text{g}} \right)^{0.34} \text{ kpc} \quad (6)$$

Using  $r_{\text{core}} > 45$  pc, we find  $\sigma/m > 0.003 \text{ cm}^2/\text{g}$  which is consistent with all known constraints to date.

Another model that could explain Eri II is ultra-light axions (e.g. González-Morales et al. (2016) and references therein). Assuming an ultra-light axion mass of  $m_a \sim 10^{-22} \text{ eV}$ , we obtain for our Eri II halo model,  $r_{\text{core}} 1.8 \text{ kpc}$  which is perfectly consistent with our minimum core size  $r_{\text{core}} > 45$  pc.

## 4.3 Implications of the initial cluster properties

The initial mass of the star cluster in the cored galaxy ( $M_{\text{cl},0} \approx 1.9 \times 10^4 M_{\odot}$ ) suggests that this star cluster resembled a young massive cluster, similar to those we see in the disc of the Milky Way (e.g. Arches, Westerlund 1, NGC 3603). The initial radius ( $r_{\text{hm},0} \approx 10 \text{ pc}$ ) is relatively large compared to these low redshift analogues, which have typical radii of a few pc (Portegies Zwart et al. 2010). We note that the model with  $r_{\text{hm},0} \approx 5 \text{ pc}$  expands up to  $r_{\text{hm}} \sim 15 \text{ pc}$  and fits the data reasonably well. Our models did not include primordial mass segregation in the cluster initial conditions. If we would have assumed that the massive stars formed more towards the centre of the cluster, it would expand more as the result of stellar mass loss (e.g. Zonoozi et al. 2017) and this could accommodate more compact initial conditions. The present day mass of stars and stellar remnants that once belonged to the cluster is  $\sim 10^4 M_{\odot}$ , or  $\sim 12\%$  of the total stellar mass in Eri II. Such a high cluster formation efficiency was also found in other dwarf galaxies with a single star cluster (Larsen et al. 2014).

## 4.4 Comparison with other work in the literature

Concurrent with our work, Amorisco (2017) have recently modelled Eri II’s central star cluster sinking under dynamical friction, finding that it cannot survive long in a cusped potential. (They also report similar results for Andromeda XXV.) Our results for Eri II are in excellent agreement with Amorisco (2017), however the key difference is that we utilise the properties of Eri II’s star cluster for the first time. Amorisco (2017) used a collisionless  $N$ -body code which is not ideal for studying the evolution of star clusters. Amorisco (2017) argues that collisional effects can be ignored in extended and faint star clusters. The initial half-mass relaxation time (Spitzer 1987) of our best-fit cluster model is  $\sim 2.2 \text{ Gyr}^9$ , and the cluster is now older than that, therefore two-body relaxation was important during the evolution of this cluster. This is further supported by the fact that models with shorter initial relaxation

<sup>9</sup> Computed assuming  $\ln \Lambda = \ln(0.02N)$  (Giersz & Heggie 1996).

timescales (i.e. smaller radii) evolve to a comparable radius and mass (see Section 4.3). This is because the properties at the present day are insensitive to the initial conditions, if two-body relaxation is important (e.g. Hénon 1961). For collisional systems evolving in a galactic potential, the density of the cluster depends only on the number of stars  $N$  and the tidal field (Gieles et al. 2011) and this is why the dark matter density can therefore be determined once  $N$  is established.

Using the evolution of the size as a fitting parameter, our study goes beyond a timing or survival argument, allowing us to obtain a direct measurement of Eri II's central DM density.

## 5 CONCLUSIONS

We have presented a new method for probing the central dark matter density in dwarf galaxies using star clusters. Low mass star clusters orbiting in the tidal field of a larger host galaxy are expected to reach an equilibrium size due to relaxation-driven expansion and the tidal pruning of high-energy escaper stars. We have used the `NBODY6DF` collisional  $N$ -body code, which includes stellar evolution and dynamical friction, to show that this is indeed the case. As a first application, we have applied our method to the recently discovered ultra-faint dwarf, Eri II. This has a lone star cluster that lies some  $\sim 45$  pc from its centre in projection. Using a grid of 200 full  $N$ -body models, we showed that models with a central dark matter core are favoured over those with a dark matter cusp. A DM core naturally reproduces the size, radial light profile and projected position of Eri II's star cluster. By contrast, dense cusped galaxy models require the cluster to lie implausibly far from the centre of Eri II ( $> 1$  kpc), with a high inclination orbit ( $i > 87.43^\circ$ ) that must be observed at a special orbital phase ( $< 3$  per cent of the orbital period).

Our models make several clear predictions that can be tested with deeper observations. If Eri II is cored, then

- the cluster can have any age older than  $\sim 7$  Gyr (vs a narrow age range of 6.5 – 8 Gyr in the cusped case);
- there are no tidal tails associated with the cluster;
- the cluster has a low concentration ( $c \sim 0.5$  vs  $c \sim 0.8$  in the cusped case).

This paper shows that extended faint star clusters can survive in the centre of a cored dark matter galaxy, making them the perfect candidate to resemble the ultra-faint objects observed in the halo of the Milky Way (for a discussion see Contenta et al. 2017). Dwarf galaxies with a DM core are more likely to be stripped by interactions with a more massive halo (e.g. Read et al. 2006b; Peñarrubia et al. 2010). Therefore, Eri II's star cluster could be the progenitor of the ultra-faint objects in the Milky Way, before they lost their host.

The presence of a dark matter core in an ultra-faint dwarf galaxy implies that either a CDM cusp was 'heated up' at the centre of Eri II by bursty star formation, or we are seeing the first unambiguous evidence for physics beyond CDM. Deeper observations should be able to measure the star formation history of Eri II and reveal the nature of dark matter.

## ACKNOWLEDGMENTS

Support for this work was provided by the European Research Council (ERC-StG-335936, CLUSTERS). MG acknowledges financial support from the Royal Society in the form of a University

Research Fellowship (URF) and an equipment grant used for the GPU cluster in Surrey. JIR would like to acknowledge support from STFC consolidated grant ST/M000990/1 and the MERAC foundation. We thank Josh D. Simon for the insightful discussions about the interpretation of the HST photometry and Denija Crnojevic for the image of Eridanus II. We are grateful to Sverre Aarseth and Keigo Nitadori for making `NBODY6` publicly available, and to Dan Foreman-Mackey for providing the `EMCEE` software and for maintaining the online documentation; we also thank Mr David Munro of the University of Surrey for hardware and software support. The analyses done for this paper made use of `SCIPY` (Jones et al. 2001), `NUMPY` (van der Walt et al. 2011) and `MATPLOTLIB` (Hunter 2007).

## REFERENCES

- Aarseth S. J., 1999, *PASP*, 111, 1333
- Aarseth S. J., 2003, *Gravitational N-Body Simulations*. Cambridge University Press, November 2003.
- Agnello A., Evans N. W., 2012, *ApJ*, 754, L39
- Ahmad A., Cohen L., 1973, *Journal of Computational Physics*, 12, 389
- Amorisco N. C., 2017, *ArXiv e-prints*
- Battaglia G., Helmi A., Tolstoy E., Irwin M., Hill V., Jablonka P., 2008, *ApJ*, 681, L13
- Bechtol K., Drlica-Wagner A., Balbinot E., Pieres A., Simon J. D., Yanny B., Santiago B., The DES Collaboration, 2015, *ApJ*, 807, 50
- Belokurov V. et al., 2007, *ApJ*, 654, 897
- Bianchini P., Renaud F., Gieles M., Varri A. L., 2015, *MNRAS*, 447, L40
- Breddels M. A., Helmi A., 2013, *A&A*, 558, A35
- Bressan A., Marigo P., Girardi L., Salasnich B., Dal Cero C., Rubele S., Nanni A., 2012, *MNRAS*, 427, 127
- Chabrier G., 2003, *ApJ*, 586, L133
- Chan T. K., Kereš D., Oñorbe J., Hopkins P. F., Muratov A. L., Faucher-Giguère C.-A., Quataert E., 2015, *MNRAS*, 454, 2981
- Claydon I., Gieles M., Zocchi A., 2017, *MNRAS*, 466, 3937
- Cole D. R., Dehnen W., Read J. I., Wilkinson M. I., 2012, *MNRAS*, 426, 601
- Collins M. L. M. et al., 2014, *ApJ*, 783, 7
- Contenta F., Gieles M., Balbinot E., Collins M. L. M., 2017, *MNRAS*, 466, 1741
- Crnojević D., Sand D. J., Zaritsky D., Spekkens K., Willman B., Hargis J. R., 2016, *ApJ*, 824, L14
- de Boer T. J. L. et al., 2012, *A&A*, 544, A73
- Dehnen W., 1993, *MNRAS*, 265, 250
- Dubinski J., Carlberg R. G., 1991, *ApJ*, 378, 496
- Dutton A. A., Macciò A. V., 2014, *MNRAS*, 441, 3359
- Evans N. W., An J., Walker M. G., 2009, *MNRAS*, 393, L50
- Fitts A. et al., 2016, *ArXiv e-prints*
- Flores R. A., Primack J. R., 1994, *ApJ*, 427, L1
- Foreman-Mackey D., Hogg D. W., Lang D., Goodman J., 2013, *PASP*, 125, 306
- Gieles M., Baumgardt H., Heggge D. C., Lamers H. J. G. L. M., 2010, *MNRAS*, 408, L16
- Gieles M., Heggge D. C., Zhao H., 2011, *MNRAS*, 413, 2509
- Gieles M., Zocchi A., 2015, *MNRAS*, 454, 576
- Giersz M., Heggge D. C., 1996, *MNRAS*, 279, 1037
- Goerdt T., Moore B., Read J. I., Stadel J., Zemp M., 2006, *MNRAS*, 368, 1073
- González-Morales A. X., Marsh D. J. E., Peñarrubia J., Ureña-López L., 2016, *ArXiv e-prints*
- Harris W. E., 1996, *AJ*, 112, 1487
- Harvey D., Massey R., Kitching T., Taylor A., Tittley E., 2015, *Science*, 347, 1462
- Hénon M., 1961, *Annales d'Astrophysique*, 24, 369; English translation: *ArXiv:1103.3499*
- Hénon M., 1965, *Ann. Astrophys.*, 28, 62; translation: *ArXiv:1103.3498 (H65)*

- Hunter J. D., 2007, Matplotlib: A 2D Graphics Environment. [Online; accessed 2016-07-21]
- Hurley J. R., Pols O. R., Tout C. A., 2000, MNRAS, 315, 543
- Hurley J. R., Tout C. A., Pols O. R., 2002, MNRAS, 329, 897
- Innanen K. A., Harris W. E., Webbink R. F., 1983, AJ, 88, 338
- Inoue S., 2009, MNRAS, 397, 709
- Inoue S., 2011, MNRAS, 416, 1181
- Jones E., Oliphant T., Peterson P., et al., 2001, SciPy: Open source scientific tools for Python. [Online; accessed 2016-07-21]
- Kaplinghat M., Tulin S., Yu H.-B., 2016, Physical Review Letters, 116, 041302
- King I. R., 1966, AJ, 71, 64
- Klypin A., Kravtsov A. V., Valenzuela O., Prada F., 1999, ApJ, 522, 82
- Koposov S. E., Belokurov V., Torrealba G., Evans N. W., 2015, ApJ, 805, 130
- Kroupa P., 2001, MNRAS, 322, 231
- Küpper A. H. W., Kroupa P., Baumgardt H., Heggie D. C., 2010, MNRAS, 407, 2241
- Laporte C. F. P., Peñarrubia J., 2015, MNRAS, 449, L90
- Larsen S. S., Brodie J. P., Forbes D. A., Strader J., 2014, A&A, 565, A98
- Larsen S. S., Strader J., Brodie J. P., 2012, A&A, 544, L14
- Li T. S. et al., 2017, ApJ, 838, 8
- Macciò A. V., Dutton A. A., van den Bosch F. C., Moore B., Potter D., Stadel J., 2007, MNRAS, 378, 55
- Madau P., Shen S., Governato F., 2014, ApJ, 789, L17
- Makino J., Aarseth S. J., 1992, PASJ, 44, 141
- Martin N. F., de Jong J. T. A., Rix H.-W., 2008, ApJ, 684, 1075
- McConnachie A. W., 2012, AJ, 144, 4
- McLaughlin D. E., van der Marel R. P., 2005, ApJS, 161, 304
- Merrifield M. R., Kent S. M., 1990, AJ, 99, 1548
- Moore B., 1994, Nature, 370, 629
- Moore B., Ghigna S., Governato F., Lake G., Quinn T., Stadel J., Tozzi P., 1999, ApJ, 524, L19
- Navarro J. F., Eke V. R., Frenk C. S., 1996a, MNRAS, 283, L72
- Navarro J. F., Frenk C. S., White S. D. M., 1996b, ApJ, 462, 563
- Nitadori K., Aarseth S. J., 2012, MNRAS, 424, 545
- Oñorbe J., Boylan-Kolchin M., Bullock J. S., Hopkins P. F., Kereš D., Faucher-Giguère C.-A., Quataert E., Murray N., 2015, MNRAS, 454, 2092
- Peñarrubia J., Benson A. J., Walker M. G., Gilmore G., McConnachie A. W., Mayer L., 2010, MNRAS, 406, 1290
- Peñarrubia J., Pontzen A., Walker M. G., Koposov S. E., 2012, ApJ, 759, L42
- Peñarrubia J., Walker M. G., Gilmore G., 2009, MNRAS, 399, 1275
- Petts J. A., Gualandris A., Read J. I., 2015, MNRAS, 454, 3778
- Petts J. A., Read J. I., Gualandris A., 2016, MNRAS, 463, 858
- Planck Collaboration et al., 2014, A&A, 571, A16
- Plummer H. C., 1911, MNRAS, 71, 460
- Pontzen A., Governato F., 2012, MNRAS, 421, 3464
- Pontzen A., Governato F., 2014, Nature, 506, 171
- Pontzen A., Read J. I., Teyssier R., Governato F., Gualandris A., Roth N., Devriendt J., 2015, MNRAS, 451, 1366
- Portegies Zwart S. F., McMillan S. L. W., Gieles M., 2010, ARA&A, 48, 431
- Read J. I., Agertz O., Collins M. L. M., 2016, MNRAS, 459, 2573
- Read J. I., Gilmore G., 2005, MNRAS, 356, 107
- Read J. I., Goerdt T., Moore B., Pontzen A. P., Stadel J., Lake G., 2006a, MNRAS, 373, 1451
- Read J. I., Iorio G., Agertz O., Fraternali F., 2017, MNRAS
- Read J. I., Steger P., 2017, ArXiv e-prints
- Read J. I., Wilkinson M. I., Evans N. W., Gilmore G., Kleyna J. T., 2006b, MNRAS, 367, 387
- Richardson T., Fairbairn M., 2014, MNRAS, 441, 1584
- Sand D. J., Spekkens K., Crnojević D., Hargis J. R., Willman B., Strader J., Grillmair C. J., 2015, ApJ, 812, L13
- Santana F. A., Muñoz R. R., Geha M., Côté P., Stetson P., Simon J. D., Djorgovski S. G., 2013, ApJ, 774, 106
- Schive H.-Y., Liao M.-H., Woo T.-P., Wong S.-K., Chiueh T., Broadhurst T., Hwang W.-Y. P., 2014, Physical Review Letters, 113, 261302
- Schneider A., Trujillo-Gomez S., Papastergis E., Reed D. S., Lake G., 2016, ArXiv e-prints
- Spergel D. N., Steinhardt P. J., 2000, Physical Review Letters, 84, 3760
- Spitzer L., 1987, Dynamical evolution of globular clusters. Princeton Univ. Press, Princeton, NJ
- Tegmark M., Zaldarriaga M., 2002, Phys. Rev. D, 66, 103508
- Tollet E. et al., 2016, MNRAS, 456, 3542
- Ural U., Wilkinson M. I., Read J. I., Walker M. G., 2015, Nature Communications, 6, 7599
- van der Walt S., Colbert C. S., Varoquaux G., 2011, The NumPy Array: A Structure for Efficient Numerical Computation. [Online; accessed 2016-07-21]
- Walker M. G., Peñarrubia J., 2011, ApJ, 742, 20
- Wang L., Dutton A. A., Stinson G. S., Macciò A. V., Penzo C., Kang X., Keller B. W., Wadsley J., 2015, MNRAS, 454, 83
- Webb J. J., Patel S. S., Vesperini E., 2017, MNRAS, 468, L92
- Wheeler C., Oñorbe J., Bullock J. S., Boylan-Kolchin M., Elbert O. D., Garrison-Kimmel S., Hopkins P. F., Kereš D., 2015, MNRAS, 453, 1305
- Wilks S. S., 1938, Ann. Math. Statist., 9, 60
- Yoon I., Lee H. M., Hong J., 2011, MNRAS, 414, 2728
- Zonoozi A. H., Haghi H., Kroupa P., Küpper A. H. W., Baumgardt H., 2017, MNRAS, 467, 758